

26 July 1966

Abstract of paper contributed to the International Symposium on Electron and Positron Storage Rings at Saclay, September, 1966.

ABSTRACT

THE DESIGN OF THE STANFORD 3-GeV ELECTRON-POSITRON  
STORAGE RING

John R. Rees

Stanford Linear Accelerator Center  
Stanford, California

The Stanford 3-GeV storage ring design has been revised to incorporate long straight sections having very small values of the vertical  $\beta$ -function at their centers. The beam reaches a minimum in vertical dimension in the center of a 5-meter-long free space for high-energy detectors. The displacement of the equilibrium orbit for off-momentum particles is zero throughout the experimental regions and is unaffected by adjustments of the interaction-region quadrupoles. The rf power provided is 1.3 megawatts. The luminosity ranges from  $1.3 \times 10^{32} \text{ cm}^{-2} \text{ sec}^{-1}$  at 3 GeV up to  $2.5 \times 10^{33}$  at 1.3 GeV. The considerations leading to the design will be discussed.

# THE DESIGN OF THE STANFORD 3-GeV ELECTRON-POSITRON STORAGE RING

John R. Rees

Stanford Linear Accelerator Center

Stanford, California

In an earlier paper, B. Richter has described the basic design criteria for a high-energy electron-positron storage ring capable of doing experiments in both electromagnetic and strong-interaction physics. This paper describes the SLAC storage-ring design based on these criteria. Considerations of couplings and some non-linear effects are covered in another paper by P. L. Morton. The design of the detectors for the SLAC storage ring is the subject of still another paper given by A. M. Boyarski.

The design of the 3-GeV electron-positron storage ring proposed to be built at the Stanford Linear Accelerator Center has been revised this year to incorporate long straight sections having very small values of the vertical beta function at their centers -- the interaction regions. In the course of the revision, all of the major systems were reviewed, and the resulting design is described in this paper. The principle contributors to this work were M. Allen, G. Fischer, E. Garwin, P. Morton, B. Richter, J. Walling and the author.

The SLAC storage ring is to be filled with electrons and positrons extracted from the two-thirds point of the two-mile linear accelerator. The positrons will be produced in a radiator at the one-third point. The SLAC linac is now in operation at beam-power levels up to 150 kilowatts average at the one-third point, corresponding to an average positron current of about 1.5 microamperes or  $10^{13}$  positrons per second, and we anticipate that these figures will be at least doubled by the time the storage ring is built. This current can be delivered at any energy at which we wish to operate the storage ring, and the pulses can be delivered in many desired time patterns, while the remaining linac output is used to service other experiments.

Fig. 1 shows the situation of the storage ring at the two-thirds point of the linac. The ring itself is covered by a thick reinforced concrete housing which provides the necessary shielding. A high bay spans the diameter of the ring between the detector areas, and the control room and electric substation about the high bay on either side in the middle of the ring. The input beams from the linac follow the Y-shaped tunnel, part of which already exists.

The main feature of our new design is the use in the magnet lattice of special insertions in which the beams are focussed to tiny vertical dimensions at the place where the bunches collide with the result that the luminosity is increased two orders of magnitude over that of our previous design. The calculated luminosity is shown in Fig. 2. The curve marked MODE A refers to the case in which all rf buckets are filled and the cross section of the beam is adjusted so that the beams are at the incoherent Courant limit,  $\Delta v_v = 0.025$ . Coherent instabilities are assumed to have been controlled by feedback. The circulating current is adjusted to keep constant radiated power; it varies as  $E^{-4}$ . The current corresponding to the maximum luminosity is 24 amperes, each beam. The beams will be kept separated by electric fields outside the interaction regions, but, because of the uncertainties about the effects of the weaker, but still important, forces between the separated bunches, we cannot be sure of achieving the luminosities calculated for MODE A in which we ignored these effects. However, we are quite confident of achieving the luminosities given by the curve labeled MODE B. In this mode, we shall fill only one bunch in each beam, and these bunches will encounter each other only at the interaction regions. In this case too, we shall adjust the beam cross sections to the incoherent limit, and the drop in luminosity at lower energies is due to aperture limitations on the beam size.

Fig. 3 shows the layout of the storage ring. The basic structure, exclusive of correcting devices, has two superperiods, and it is symmetric about the centers of the detectors. Each superperiod comprises five separated-function AG cells and a set of special elements belonging to the insertion. Many of the parameters are listed on Fig. 3.

#### The Magnet

The magnet gap was chosen to be 10 cm high by 38 cm wide. In choosing the width, we considered primarily the damping times at 3 GeV, the repetition rate of the SLAC linac and the cost of the magnets. The 38-cm width enables us to inject every other pulse without loss of particles from the preceding injected pulse. A considerably wider pole would be required to facilitate filling on every pulse at the 300 pps repetition rate of the linac, and, in view of the short filling time at 3 GeV (1 second), the extra cost was not deemed to be warranted.

The gap height was chosen to allow reasonable space for accommodating large currents with separated orbits. A substantial gap height is of paramount importance for large currents because of the incoherent limit.

The radial and vertical betatron frequencies are adjustable. The basic design criteria imposed on the lattice were the following:

- (1) That the ring be tunable, so that the best operating point could be found, and, in particular, so that a point just above an integral resonance can be reached in operation;
- (2) That the value of the vertical beta function at the interaction region be adjustable in operation ; and
- (3) That a value of the vertical beta function at the interaction region as small as 5 cm be reached.

These criteria are all met. The tunes given on Fig. 3 are typical tunes for injection. Electric quadrupoles (EQ) are included in the design to split the betatron frequencies of the electron and positron beams to weaken the tendency for two-beam coherent oscillations. Electronic feedback systems are also planned for this purpose.

Our approach to designing the lattice was first to design a symmetric AG cell and then to design an insertion with a long straight section to be inserted at a symmetry point of the cell. Then we put the machine together out of these pieces.

The betatron functions of the cell are shown in Fig. 4. The structure of the cell and some of the parameters are also shown at the top of the figure. The bending magnets are rectangular; they produce no radial focusing. Consequently, the radial radiation-damping rate is equal to the vertical damping rate. The straight section in the cell, which is to be used for a variety of things already planned and, probably, an even greater variety not yet thought of, is three meters long. In this connection, it is worth mentioning that the circumference factor of our ring, the ratio of the bending radius to the gross radius, is 0.38, quite small by synchrotron standards. Although costs could be reduced by building a smaller ring with a larger circumference factor, we feel that doing so would be a false economy because of the amounts of space needed for the vacuum system, the electrodes, the rf system, the

correcting systems, and, most important, the ad hoc devices which will ultimately be needed to achieve productive operation.

The betatron functions for the insertion are shown in Fig. 5. The center of the abscissa is the interaction region and  $\beta_v = 5$  cm there in the case plotted. The value of  $\beta_v$  at the interaction region is variable. The origin of the abscissa in Fig. 5 is, for convenience, a symmetry point of the cell; it matches to the end of the abscissa of Fig. 4.

The insertion was designed in two steps. The section from  $Q_1^+$  to the end of the third bend (BB) from the left is a "momentum-cancelling" section. By means of this set of elements, all of which are standard cell components, the displacement of equilibrium orbits for off-momentum particles is reduced to zero throughout the central region of the insertion. This done, adjustments of the beta functions at the interaction region have no effect on the displacement of off-momentum equilibrium orbits outside the insertion. The momentum-cancelling section was simple to design, and, since large values of both beta functions are required at  $Q_1$ , the space required cost nothing.

Following the momentum-cancelling section is a singlet-drift-doublet combination for producing the small vertical beta at the interaction region. No effort was made to specify the radial beta function. It is possible to omit the singlet  $Q_1$  and produce a specified value of  $\beta_v$ , but then all parameters are completely fixed, and the value may not be adjusted without moving magnets.  $Q_1$  provides for this adjustment in operation. This feature was originally deemed desirable for injection, although our present opinion is that it will be unnecessary. As beta is adjusted, the tune, of course, changes, but not wildly. For example, in the change from  $\beta_v = 7$  cm to  $\beta_v = 111$  cm, the vertical tune changes by  $-0.05$  and the radial tune by  $+0.36$ . These changes can easily be compensated by tuning the cells.

The choice of 5 cm for the minimum value of  $\beta_v$  at the interaction region was made on the basis that the transverse momenta in the beam should not contribute more to the errors in the determination of the momenta of the reaction products than the measurement errors in the detector.

### The Injection System

The injection system is shown in Fig. 6. The positrons and electrons are produced in a radiator at the one-third point of the linac and extracted by a pulsed magnet from the two-thirds point. The transport system to the

storage ring consists of one achromatic system through which both positrons and electrons pass to the splitter magnet followed by two separate achromatic systems, one for each kind of particle, to carry the particles to the deflectors. The deflectors, which are septum magnets, are located symmetrically in the ring.

The fast-orbit-perturbation method of injection is used. Two kicker magnets (perturbators) produce an orbit distortion which brings the stored beams near the septum-type deflection magnets when a new pulse is to be injected. After the new pulse is in the ring, the kickers are turned off in about three revolutions during which the new particles, executing a coherent radial betatron oscillation, do not return to the vicinity of the deflectors. This method was selected over the non-septum pulsed-deflector method in order to gain vertical aperture in the injection channel (without losing horizontal aperture in the ring) in case we have to inject particles onto vertically separated orbits. The deflector magnets are, in fact, pulsed, but only to reduce the duty cycle in the interest of thinning the septum; they are pulsed slowly compared to the kickers.

A unique feature of the injection transport system is the use of the double-gapped alternating-gradient magnets in the part of the transport system common to both kinds of particles. These magnets, shown at the top of Fig. 6, are used in doublets in the first achromatic bend. Electrons and positrons pass through opposite sides of the AG doublets and through the middle of the field triplet (quadrupoles), and they can be handled on alternate pulses without magnet switching. Thus we have the capability of filling with both particles at the same rate and on interlaced pulses if it proves necessary in order to control instabilities.

The filling time for 1 ampere in each beam at 3 GeV is calculated to be 1 second, and for 24 amperes in each beam, required at maximum luminosity (See Fig. 2.), about 5 minutes. The SLAC linac also has the capability to operate with very short pulses at higher currents, the total charge in the pulse remaining nearly constant. Thus a single bunch in each beam can be filled to the same circulating current with little increase in filling time. These high filling rates are, of course, crucial to the high luminosity of the SLAC design at low energies.

### The Vacuum System

The calculated gas load in the vacuum system is based on an extrapolation from experience with the Princeton-Stanford 200-MeV storage rings according to the law

$$\text{Gas production rate} \propto \gamma^{1/2} \rho^{-1/2} I,$$

where  $\gamma$  is the relativistic factor,  $\rho$  is the radius of curvature and  $I$  is the circulating current, but reduced a factor of five owing to the use of the aluminum vacuum chamber described below.

The bending-magnet vacuum chamber is shown in cross section in Fig. 4. The chamber will be formed by extruding aluminum with the cooling and bake-out-fluid channels as shown. The synchrotron radiation will be absorbed directly on the chamber wall, which will be corrugated after extrusion so that the radiation will strike at more nearly normal incidence, on the average. The use of aluminum is advantageous in two ways. The electron desorption coefficients for aluminum are about a factor of two less than those for stainless steel or copper, and photoelectric yield is down from that of those two metals by a factor of two or more. The less oblique angle of incidence will reduce the photoelectric yield relative to that of the Princeton-Stanford rings by a factor of three or four. We estimate conservatively that the present design reduces gas loads by a net factor of five with respect to a flat stainless steel surface.

For clearing and separating field electrodes, we have adopted the Frascati design using an array of wires as shown on Fig. 5. The tolerances on field gradients to avoid intolerable couplings between horizontal and vertical motion are stringent, but they can be met with these structures. These tolerances are discussed at this meeting by P. L. Morton in another paper.

In our earlier storage-ring design, a distributed cryogenic pumping system was proposed to handle the gas load. In the present design, the cryogenic system has been eliminated for two reasons: first, the use of the corrugated aluminum radiation catcher reduces the gas load, and, second, the use of shorter bending magnets and the wire electrodes increases the conductance of the chamber between pumps. The locations of the pumps, 1000-liter/second ion getter pumps, are shown in Fig. 3; the total pumping speed is 54,000 liters/sec.

A computer calculation of the pressure profile has been made, and the average partial pressures are given in Fig. 7. The net beam half-life due to gas bremsstrahlung is 4.3 hours at 3 GeV.

### The Radiofrequency System

The radiofrequency chosen is 50 MHz which corresponds to a harmonic order of 36. At frequencies of the order of the orbital frequency, 1.39 MHz, the advantage of the low-beta interaction region is vitiated and it is very difficult to avoid ceramic gap insulators with high voltages across them. The highest frequencies considered, around 500 MHz, lead to a more costly system and, we feel, are dangerous from the point of view of instabilities, both coherent and incoherent. 50 MHz seemed an excellent compromise.

The layout of the system is shown on Fig. 3. There are six accelerating cavities, each with its own 210-kilowatt rf amplifier. A sketch of the (currently preferred) cavity is shown in Fig. 8, along with some of the relevant parameters of the rf system. The total deliverable power from the amplifiers is 1.3 megawatts. The synchrotron radiation loss at 3 GeV is 0.563 MeV/turn, so the power absorbed by two 1-ampere beams at that energy is 1.13 megawatts. We plan to dissipate 1/10 that much power in the system. An interesting feature of the cavity, which is an evacuated aluminum structure, is the counterflow heat exchanger to remove the heat produced in the center conductors. The heat exchanger is designed conservatively to handle 15 kilowatts, corresponding to a total peak voltage of 880 kilovolts on the system, the design figure for 3 GeV. The cavity can probably be operated at considerably higher levels.

To ensure the stability of the beam-cavity system against coherent phase oscillations, the cavities will be equipped with servo-controlled tuning and matching networks. The whole spectrum of cavity resonances will also be studied, and steps will be taken to eliminate dangerous higher resonances before the final six cavities are fabricated. Also, the rf amplifiers will be Class B with wide-band amplitude and phase modulation capabilities to facilitate the use of feedback.

### Correcting Devices

Fig. 3 shows, interspersed in the magnet lattice, several correcting devices. Sextupole magnets, some of which are not shown, will be used to

cancel the dependence of betatron frequency upon momentum and to cancel the driving terms for the third order non-linear resonances. The sextupole fields are the topic of another paper given at this meeting by P. L. Morton.

Electric quadrupoles were mentioned above.

Skewed quadrupoles may be needed to correct linear couplings caused, for example, by the detector.

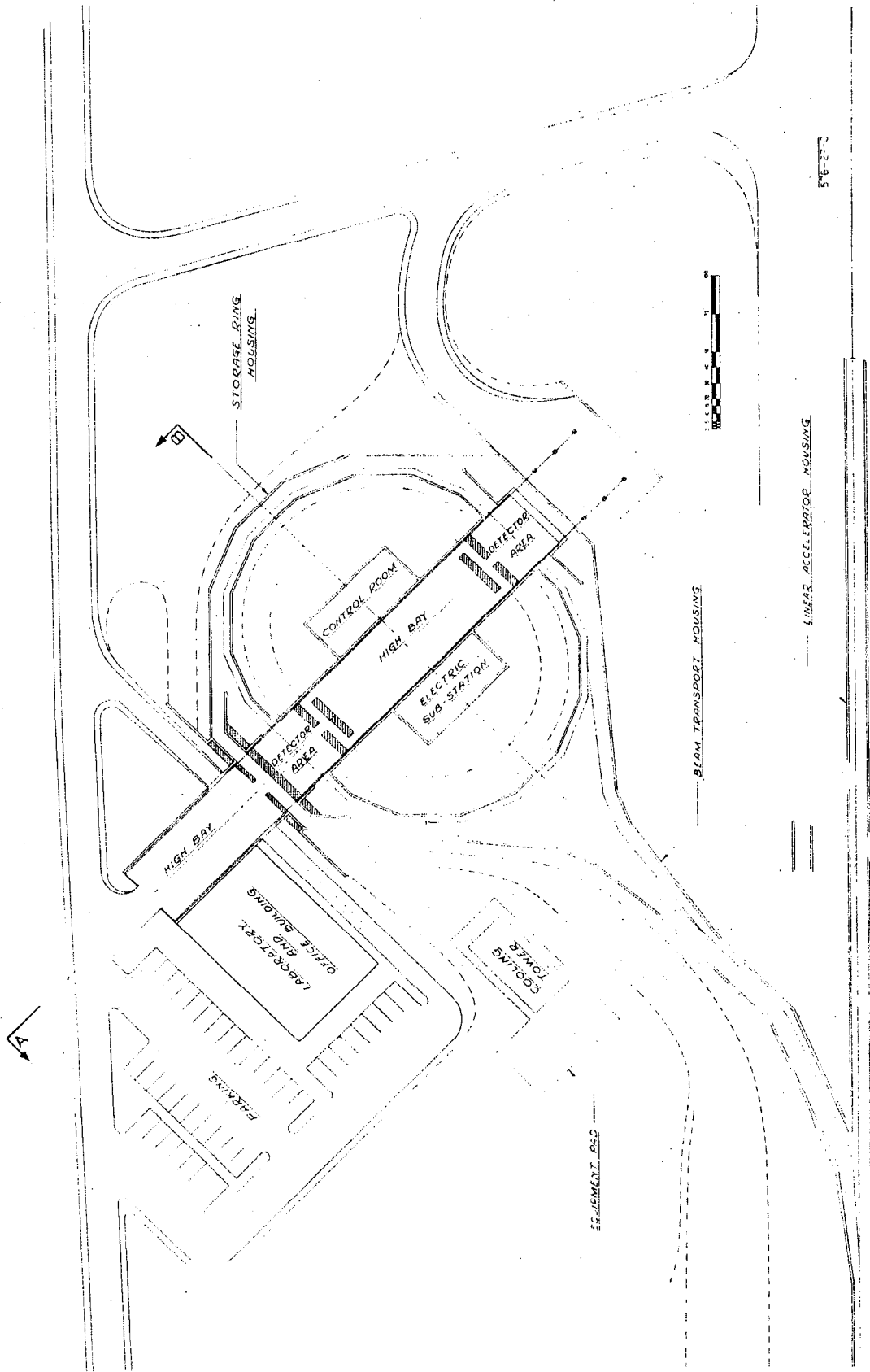
Broad-band feedback systems are planned to damp coherent oscillations.

#### Beam Lifetime

The two dominant effects on beam lifetime are bremsstrahlung on the residual gas and the Touschek effect. The latter becomes important in the SLAC storage-ring design because of the low-beta interaction region where the bunch volume is small. The Touschek lifetimes are 7.5 hours at 3 GeV and 2.5 hours at 1 GeV. The total lifetimes are 2.3 hours at 3 GeV and 1.3 hours at 1 GeV.

Figure Captions

- Fig. 1 Plan view of building layout at two-thirds point of time.
- Fig. 2 Computed luminosities.
- Fig. 3 Component layout of storage ring.
- Fig. 4 Beta functions of the normal cell.
- Fig. 5 Beta functions of the insertion.
- Fig. 6 Injection system including beam transport from the linac.
- Fig. 7 Vacuum chamber cross section in a bending magnet.
- Fig. 8 Evacuated radiofrequency cavity.



5-6-27-0

Fig. 1

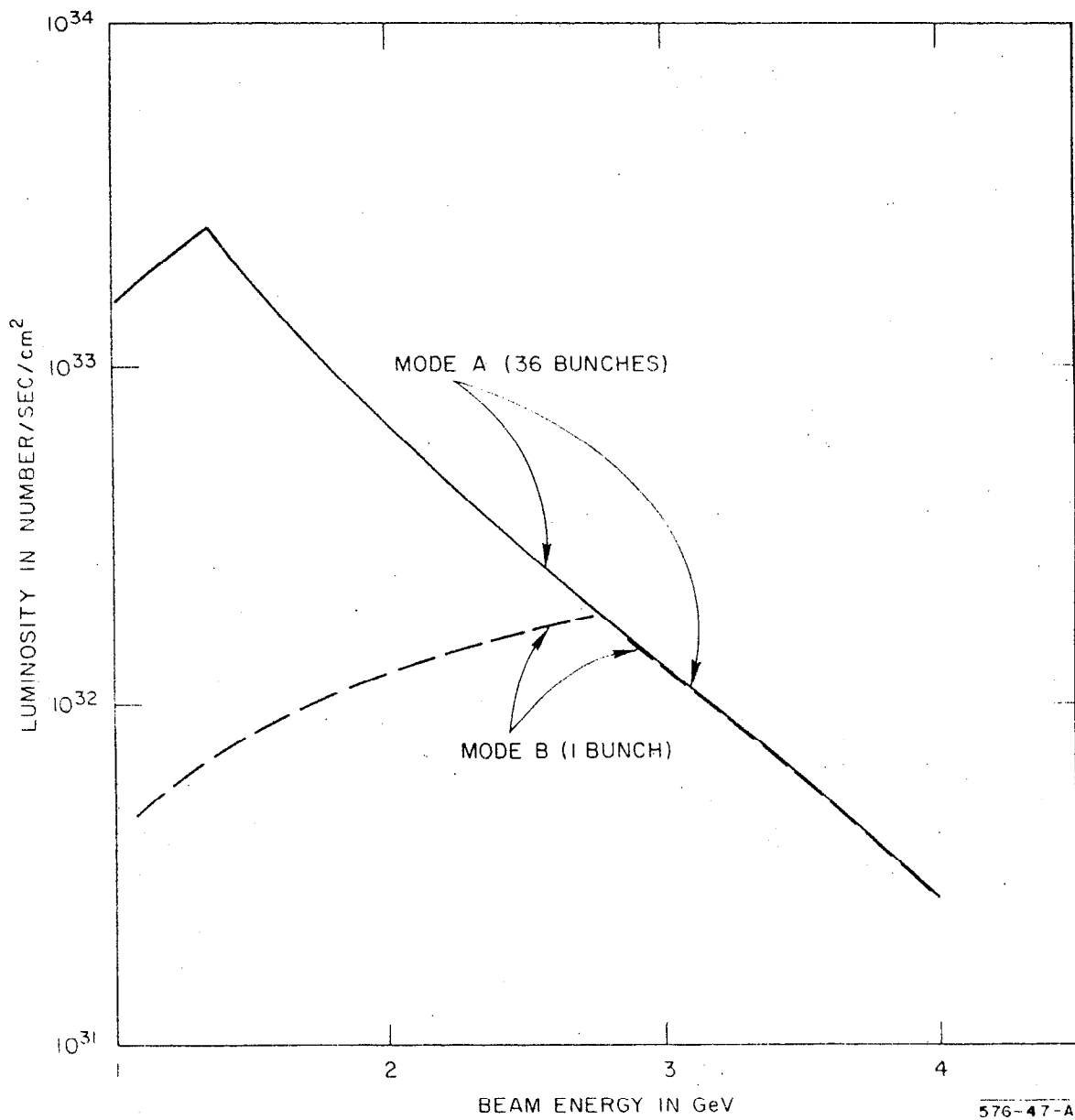


Fig. 2

Magnet

Number of normal cells	10
Number of superperiods	2
Number of insertions	2
Mean radius	112.79 ft.
Bending magnet field	7,859 kilogauss (at 3 GeV)
Bending magnet gap	4.0 inches
Bending magnet pole width	15 inches
$Q_r$	5.25 (adjustable)
$Q_v$	5.15 (adjustable)
$Q_{e^+ - e^-}$	0 - 0.1
Momentum compaction	0.046
Rev. Frequency	1.39 MHz
Wt. of iron tons	280 (bending magnets)
	76 (quadrupoles)
Wt. of copper tons	26 (bending magnets)
	15 (quadrupoles)
Magnet Power	1500 kW bending magnets
	1700 kW quadrupoles

Beam Properties at 3 GeV

Circulating current	1.0 amp (each beam)
Synchrotron radiation loss	0.563 MeV/turn
Synchrotron phase angle	140°
R. F. voltage (peak)	880 keV
Quantitative illumination lifetime	> 10 <sup>6</sup> sec
Vertical damping time	7.2 millisecc
Radial damping time	7.2 millisecc
Bunch length	2 $\sigma_z$ = 25 cm
Beam lifetime	2.3 hrs
Filling time	1 second
Luminosity	1.3 x 10 <sup>32</sup> (at 3 GeV)

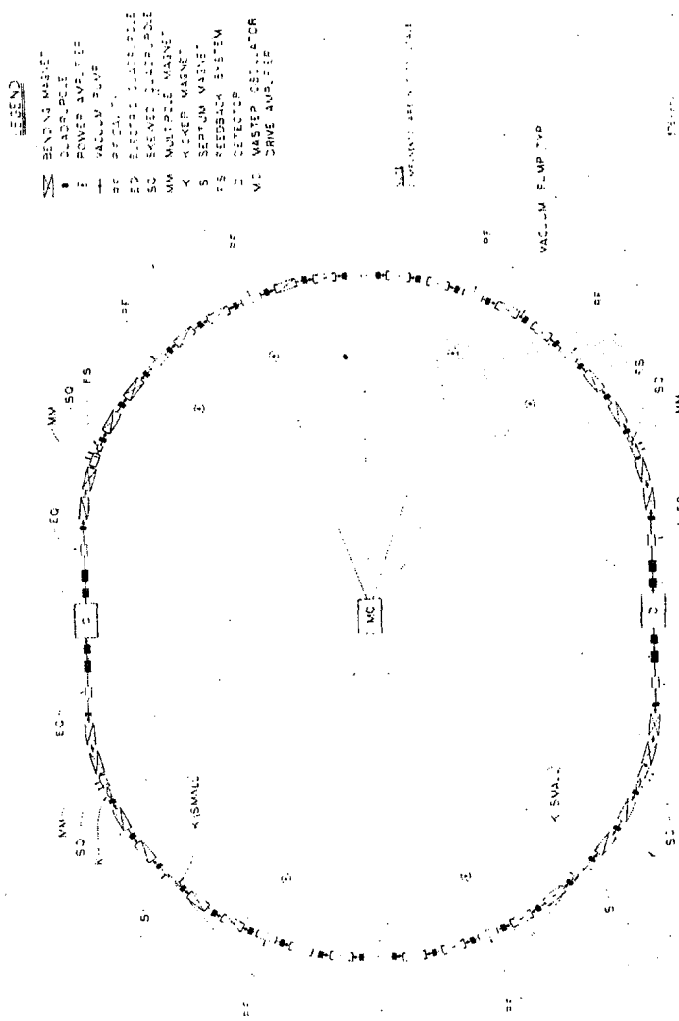


Fig. 3

Field or Gradients at 3 GeV

Component	Type of Component	Field or Gradients at 3 GeV
QD	Defocusing Quadrupole	- 604 gauss/cm
BB	Bending Magnet (n=0)	7.859 kilogauss
QF	Focusing Quadrupole	324.4 gauss/cm

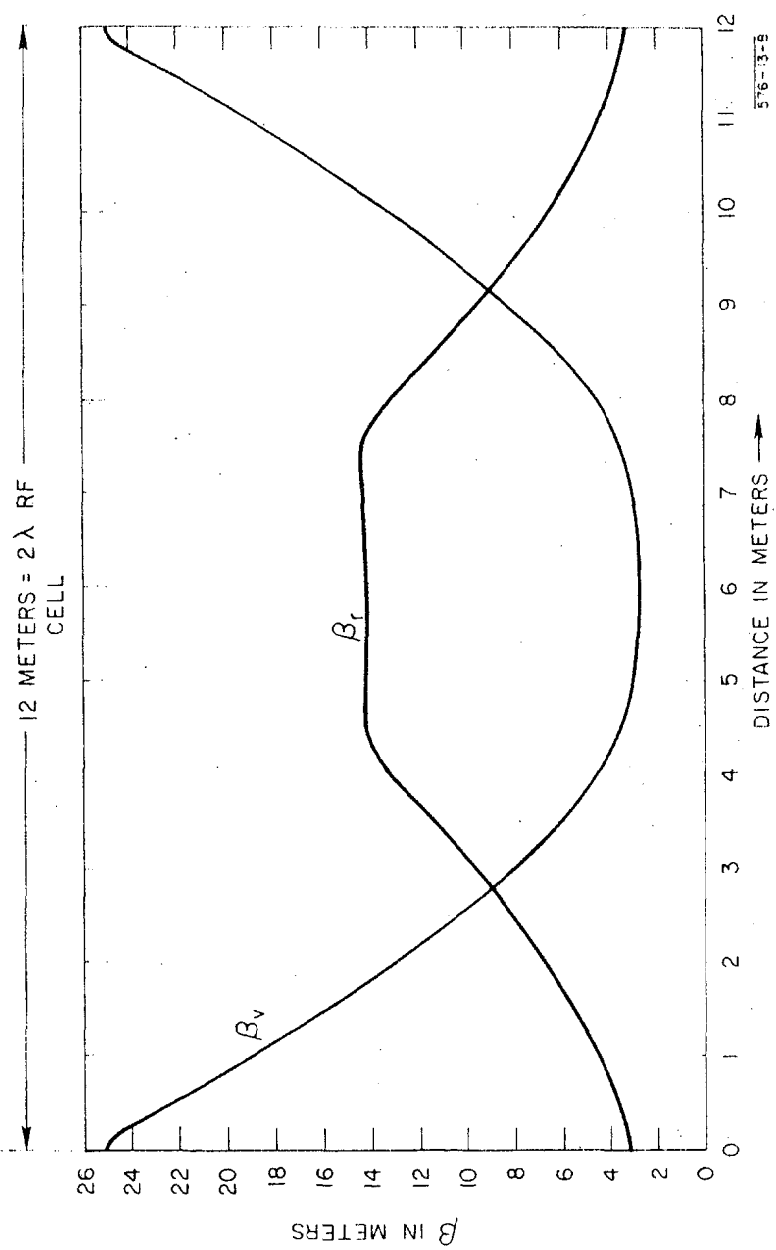


Fig. 4

<u>Component</u>	<u>Type of Component</u>	<u>Field or Gradients at 3 GeV</u>
QD	Defocusing Quadrupole	- 604 gauss/cm
BB	Bending Magnet (n-o)	7.859 kilogauss
QF1	Focusing Quadrupole	669.9 gauss/cm
Q1	Defocusing Quadrupole	- 32.6 gauss/cm
Q2	Focusing Quadrupole	372.2 gauss/cm
Q3	Defocusing Quadrupole	- 676.9 gauss/cm

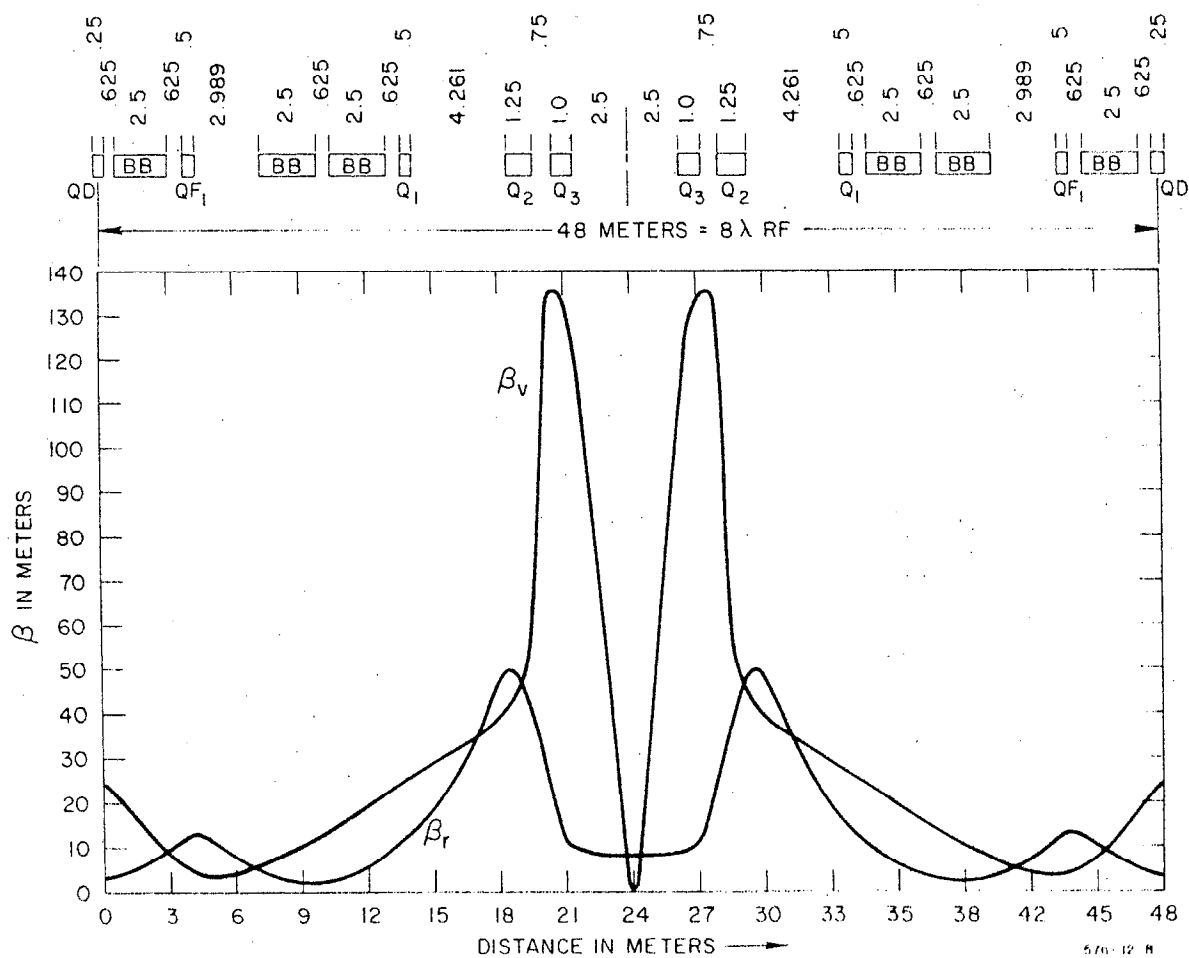
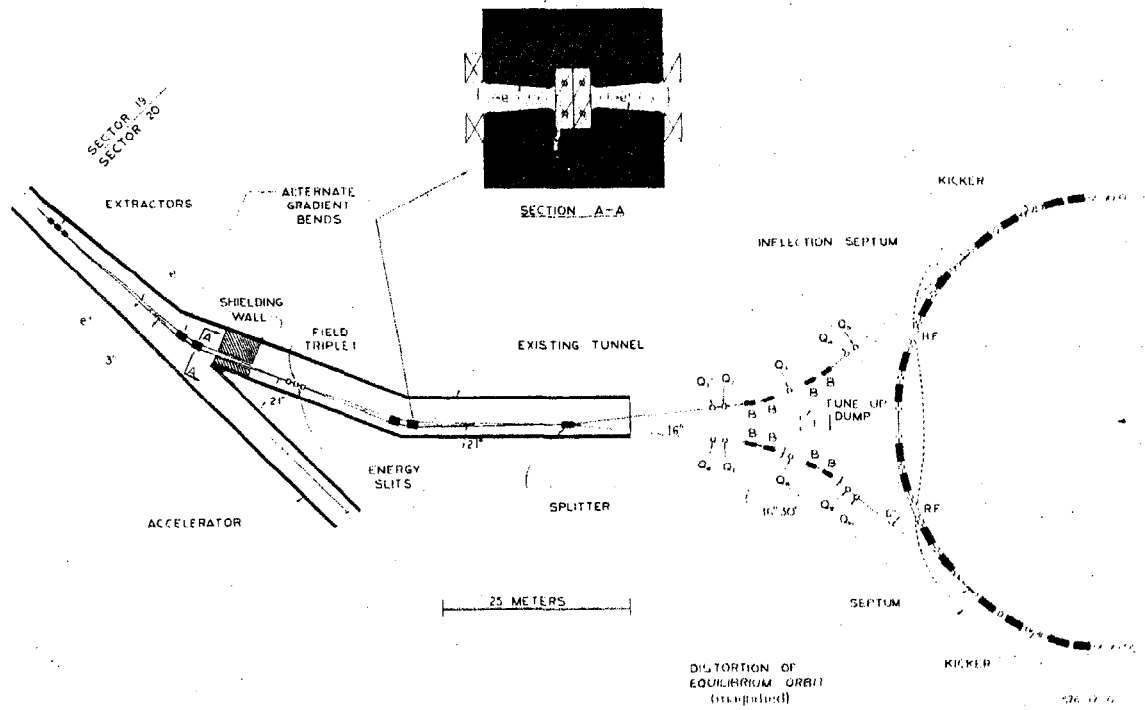


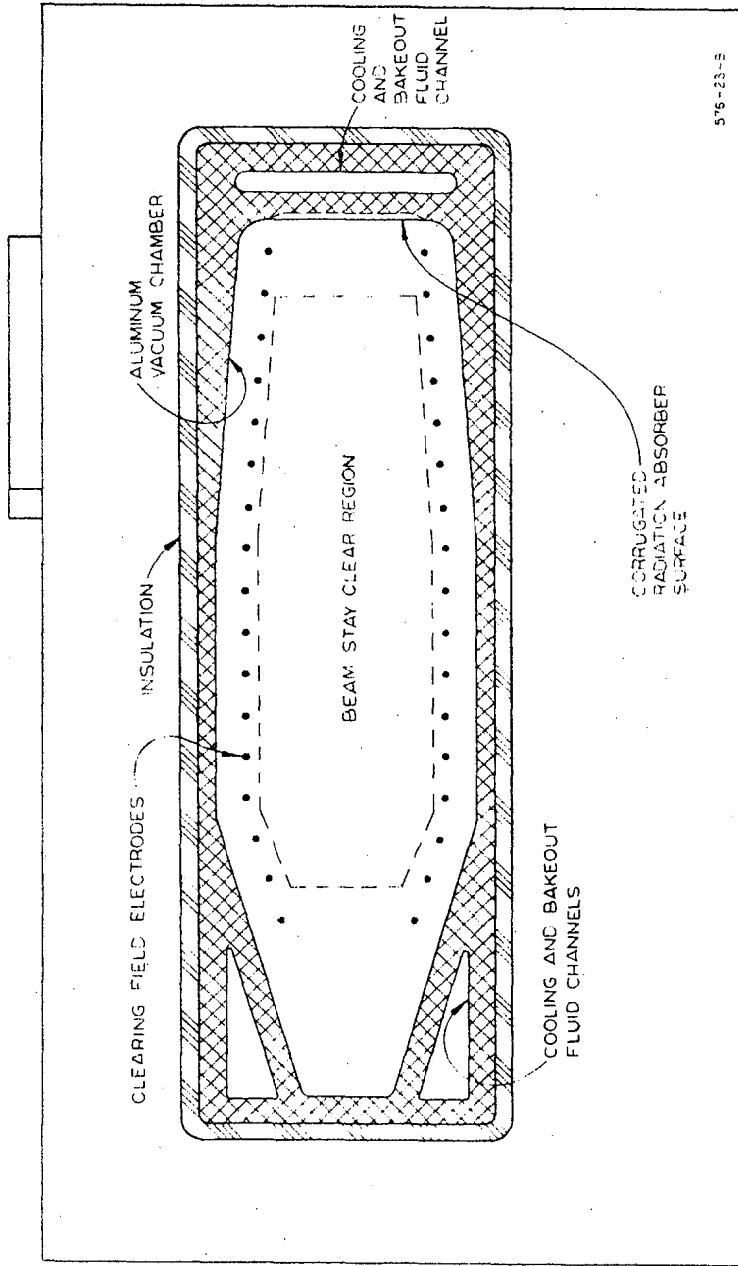
Fig. 5

Parameters of Injection Transport System at 3 GeV



No. of Magnets Required	Magnet Designation	Length Meters	Field kgauss	Gradient gauss/cm	Max Aperture	
					vert. cm	horiz. cm
3	Extractor	.85	2.0	0	.6	1.0
4	Gradient Bends	1.5	12.2	$n = 8.8$	1.6	5
2	Field Triplet	.37		-900	.4	17
1		.75		+860	.4	17
1	Splitter	1.5	6.9	0	.4	.4
4	Q <sub>1,5,6,10</sub>	.5		+720	1.6	4
4	Q <sub>2,4,7,9</sub>	.5		-630	1.6	4
2	Q <sub>3,8</sub>	.5		+700	1.6	1.2
8	Bends	1.5	9.6	0	2.0	1.5
2	Septum	1.0	10.4	0	.2	.2

Fig. 6



Vacuum System

Material

Aluminum, type 6061-T4  
and Stainless steel, type 304L

Pumping Speeds

- Ion-getter system
- 51,000 liters/sec for CO<sub>2</sub>, N<sub>2</sub>, etc.
- 192,000 liters/sec for H<sub>2</sub>
- 21 x 10<sup>-9</sup> torr H<sub>2</sub>
- 5 x 10<sup>-9</sup> torr CO
- 2 x 10<sup>-9</sup> torr CO<sub>2</sub>

Vacuum System Technical Parameters

Fig. 7

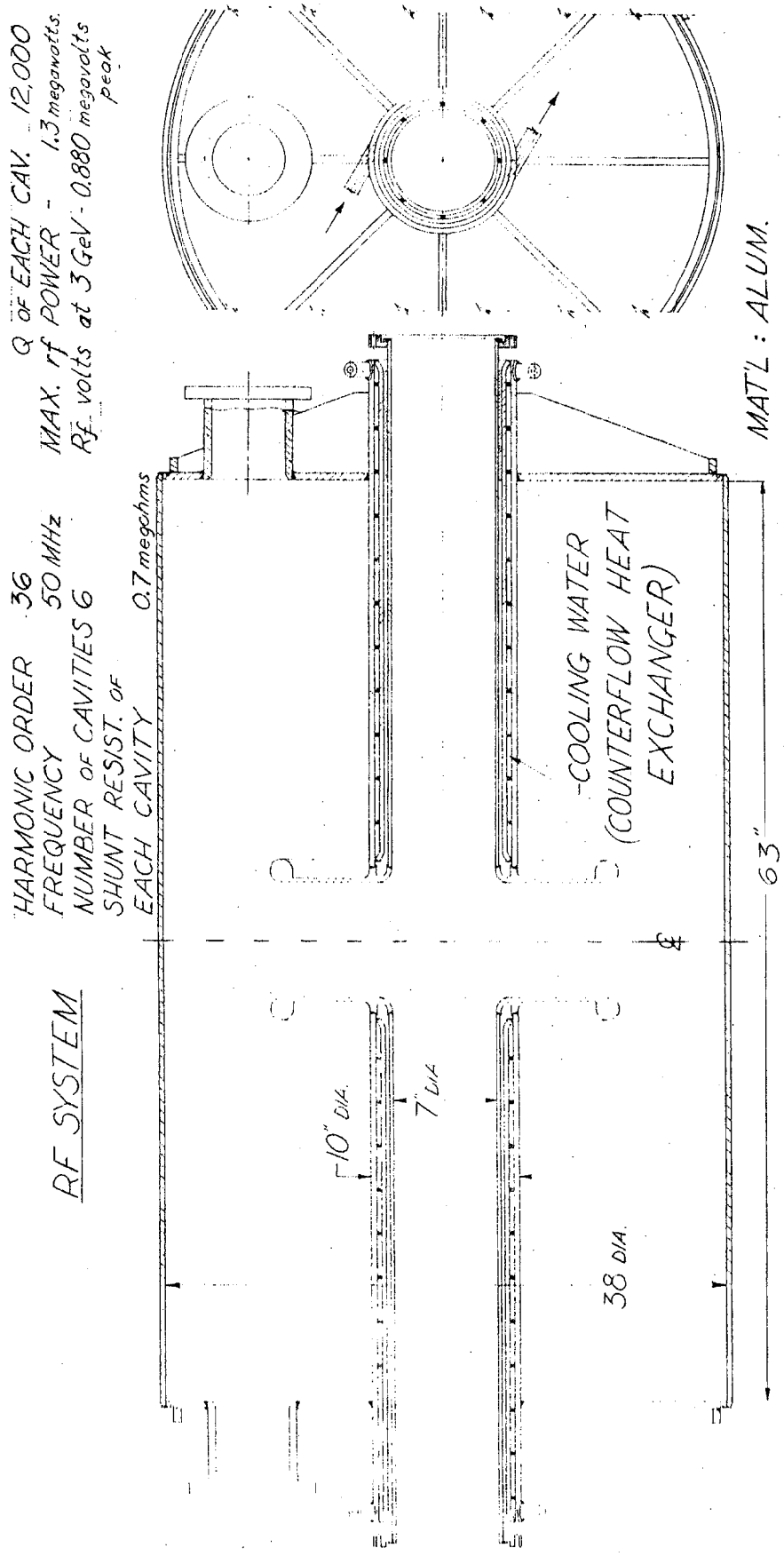


FIG. 8